Draft version September 19, 2018
Typeset using LaTeX **twocolumn** style in AASTeX62

Predicting the rotational constraint in stratified, compressible convection

Evan H. Anders,[1,2] Cathryn M. Manduca,[2] Benjamin P. Brown,[1,2] and Jeffrey S. Oishi[3]

[1] *Dept. Astrophysical & Planetary Sciences, University of Colorado – Boulder, Boulder, CO 80309, USA*
[2] *Laboratory for Atmospheric and Space Physics, Boulder, CO 80303, USA*
[3] *Department of Physics and Astronomy, Bates College, Lewiston, ME 04240, USA*

(Received September 19, 2018; Revised September 19, 2018; Accepted September 19, 2018)

Submitted to ApJ

ABSTRACT

Here we study numerical simulations of stratified, compressible convection in a rotational f-plane geometry. We discuss how the rotational constraint, measured by the Rossby number (Ro), can vary as a function of the convective driving, measured by the Rayleigh number (Ra). We define a relationship between Ra and the Taylor number (Ta) which we call the Predictive Rossby Number, $\mathcal{P}_{\rm Ro} = {\rm Ra} \,/\, {\rm Ta}^{3/4}$, and we find that the Ro remains roughly constant across orders of magnitude of Ra when $\mathcal{P}_{\rm Ro}$ is fixed.

Keywords: convection — happy caterpillars

1. INTRODUCTION

Convection under the influence of rotation has been studied in great detail in recent decades. In the incompressible boussinesq case, numerous authors have studied rotating convection in both laboratory and numerical settings. The behavior of the heat transport in these systems has been the focus of many of these studies, particularly the difference of behavior of heat transport in rotationally-constrained and unconstrained regimes (King et al. 2009; Zhong et al. 2009; Stevens et al. 2009; Julien et al. 2012). Studies of both laboratory (cite, cite) and numerical (cite, cite) experiments coincide well in these regimes.

More complicated experiments of rotational convection are often conducted using numerical tools in spherical geometries. Often these studies aim to gain insight into the solar dynamo (Glatzmaier & Gilman 1982; Busse 2002; Brown et al. 2008, 2010, 2011; Augustson et al. 2012; Guerrero et al. 2013; Käpylä et al. 2014). Numerous interesting phenomenological discoveries have been made in such studies, but they often employ very different degrees of rotational constraint, and their basic system behavior often differs significantly from the Sun. For example, dynamo simulations often produce antisolar differential rotation profiles at nominally solar values of rotational constraint.

In recent years, helioseismic imaging of flows in the Sun have suggested that power in large-scale convective motions is much lower than convective simulations and mixing length theory predict (Hanasoge et al. 2012; Greer et al. 2015). This suggests that either convection is not driven deep in the solar convection zone or its motions are masked before they reach the surface by some process. It has been suggested that the interior convection zone is rotationally constrained, and that this behavior is reducing low wavenumber power at the surface. The recent simulations of Featherstone & Hindman (2016) and the observations of Greer et al. (2016) support this hypothesis. The degree of rotational constraint under which convective flows occur can greatly change the character of the resultant situation, and so in the case of astrophysical contexts (solar studies such as those mentioned above and also planetary studies such as e.g., Soderlund et al. (2015); Aurnou & King (2017)), it is important to study convection in the same rotational regime as the astrophysical object of interest in order to meaningfully understand results.

One difficulty in studying rotational convection is that it is often unclear from input parameters whether or not the resulting convective state will be rotationally constrained. In Anders & Brown (2017) (hereafter AB17),

Corresponding author: Evan H. Anders
evan.anders@colorado.edu

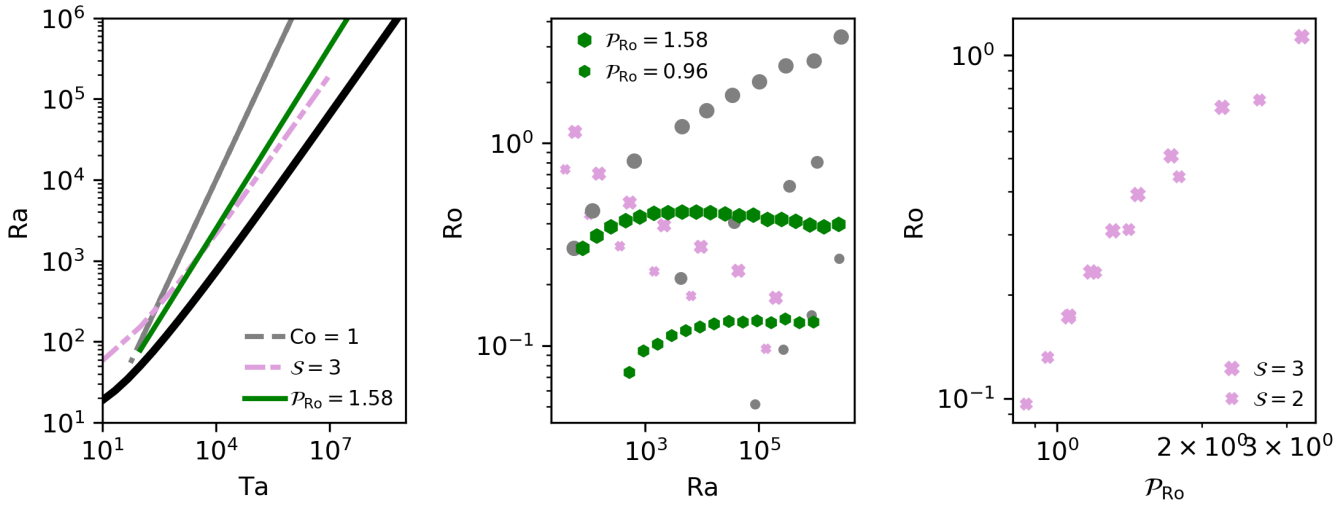

Figure 1. (a) The critical Rayleigh number, as a function of the Taylor number, is plotted as a solid black line. Paths of constant Convective Rossby Number (red dashed line), constant supercriticality (orange dashed line), and $\mathcal{P}_{\rm Ro}$ (blue solid line) are shown through parameter space. (b) Evolved Ro is plotted vs. Ra along multiple constant $\mathcal{P}_{\rm Ro}$ paths and the constant Co and $\mathcal{S}$ path shown in (a). After a sharp increase at low Ta, the evolved Rossby number flattens out and stays nearly constant across orders of magnitude of Ta. (c) At low Ro, we find that Ro $\propto \mathcal{P}_{\rm Ro}{}^{X}$.

we studied non-rotating, hydrodynamic, compressible convection. We showed how the evolved Reynolds number, Peclet number (Re and Pe, two measures of turbulence in the evolved state), and Mach number (Ma, the ratio of flow speed to the local sound speed) of the convective solution can be specified through a properly constructed reference atmosphere. Upon the inclusion of rotation, a fourth dynamical measure of the solution becomes meaningful: the Rossby number (Ro, the ratio of advective dynamics to rotational constraint). Low Ro flows are rotationally constrained, while high Ro flows are not. While the literature contains a wealth of information regarding how the magnitude of rotation affects the heat transport characteristics of convection, we find no work which links the rotational constraint of evolved solutions with input parameters.

In this work, we extend the study of AB17 to rotationally-influenced, f-plane polytropic atmospheres, as have been previously studied by e.g., Brummell et al. (1996, 1998); Calkins et al. (2015). Our goal is to determine how the input parameters which we studied previously couple with a new input parameter, the Taylor number (Ta, Julien et al. (1996)), which sets the magnitude of the rotational vector. In section 2, we describe our atmosphere, numerical experiment, and paths through parameter space. In section 3, we present the results of our experiments and in section 4 we offer concluding remarks.

2. EXPERIMENT

We study fully compressible, stratified convection under precisely the same atmospheric model as we previously did in AB17, but here we have included rotation. We study polytropic atmospheres with $n_\rho = 3$ density scale heights and a superadiabatic excess of $\epsilon = 10^{-4}$ such that flows are at low Mach number. As in previous work (Julien et al. 1996; Brummell et al. 1996), we study a domain in which the gravity, $\boldsymbol{g} = -g\hat{z}$, and rotational vector, $\boldsymbol{\Omega} = \Omega\hat{z}$, are antiparallel.

We evolve the velocity ($\boldsymbol{u}$), temperature (T), and log density ($\ln\rho$) according to the Fully Compressible Navier-Stokes equations in the same form presented in AB17, with the addition of the Coriolis term, $2\boldsymbol{\Omega}\times\boldsymbol{u}$, to the left-hand side of the momentum equation.

The kinematic viscosity (ν), thermal diffusivity (χ), and strength of rotation (Ω) are set at the top of the domain by the Rayleigh number (Ra), Prandtl number (Pr), and Taylor number (Ta),

$$\mathrm{Ra} = \frac{gL_z^3\Delta S/c_P}{\nu\chi}, \quad \mathrm{Pr} = \frac{\nu}{\chi}, \quad \mathrm{Ta} = \left(\frac{2\Omega L_z^2}{\nu}\right)^2, \qquad (1)$$

where L_z is the depth of the domain, $\Delta S = \epsilon n_\rho/m$ is the specific entropy difference between $z = 0$ and $z = L_z$, and the specific heat at constant pressure is c_P. Throughout this work we set Pr = 1.

As Ta increases, the critical value of Ra at which convection onsets, $\mathrm{Ra}_{\rm crit}$, also increases (see the black line in Fig. 1a). The linked nature of these crucial control parameters makes it difficult to predict the rotational constraint of the evolved fluid flows for a given set of input parameters. In this work, we will explore three

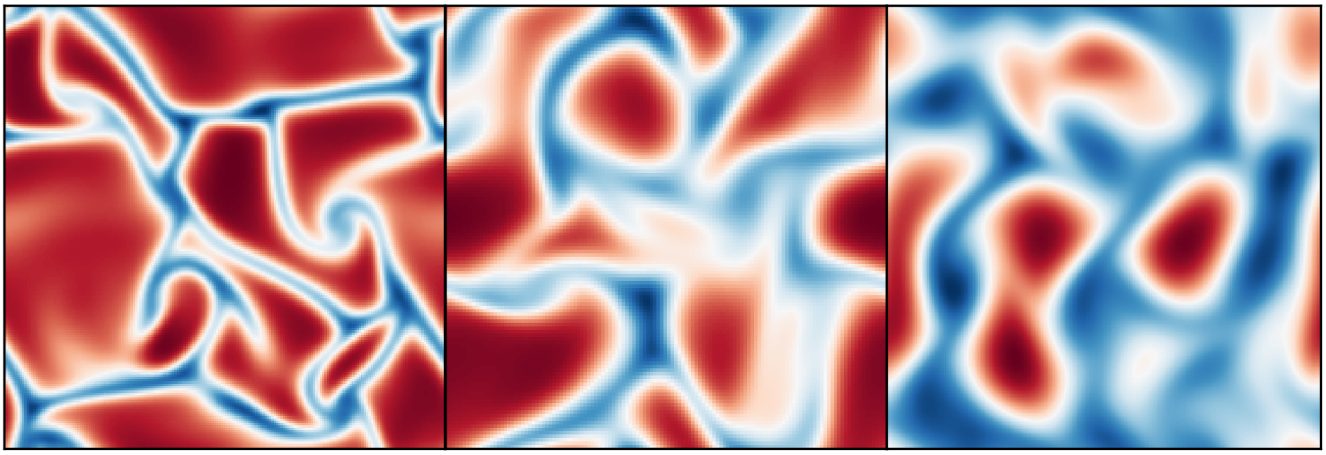

Figure 2. Here's some pretty plots, we'll figure out what we plot later.

paths through Ra-Ta space:

$$\mathrm{Ra} = \begin{cases} \mathcal{S}\,\mathrm{Ra_{crit}(Ta)}, & \text{(I)} \\ \mathrm{Co^2 Pr\ Ta}, & \text{(II)} \\ \mathcal{P}_{\mathrm{Ro}}\,{}^2\mathrm{Pr\ Ta^{3/4}} & \text{(III)}. \end{cases} \tag{2}$$

Paths on constraint I are at constant supercriticality, $\mathcal{S}$ (orange dash-dot line in Fig. 1a). Paths on constraint II are at a constant value of the classic "Convective Rossby number" (Co), which has been used frequently over the past two decades, and is intended to predict the rotational constraint of the evolved solution (red line in Fig. 1a; Julien et al. (1996); Brummell et al. (1996)). Paths on constraint III set constant a ratio which we call the "Predictive Rossby Number" ($\mathcal{P}_{\mathrm{Ro}}$). These paths follow contours of $\mathrm{Ta}^{3/4}$, and to our knowledge have not been well-explored in the literature (blue solid line in Fig. 1a).

In this work, our goal is to study the magnitude of the rotational constraint along each path defined in Eqn. 2. We will quantify rotational constraint using the Rossby number,

$$\mathrm{Ro} = \frac{|\nabla \times \boldsymbol{u}|}{2\Omega}. \tag{3}$$

As Ta increases, the wavenumber of convective onset, k_{crit}, also increases. We study 3D cartesian convective domains with horizontal extents of $x, y = [0, 4(2\pi/k_{\mathrm{crit}})]$. We evolve our simulations using the Dedalus[1] pseudospectral framework, and our numerical methods are identical to those presented in AB17.

3. RESULTS & DISCUSSION

In Fig. 1a, we display the value of the critical Rayleigh number ($\mathrm{Ra_{crit}}$) as a function of the Taylor number (Ta). We found these critical values through the use of a linear instability analysis. We plot a sample path for each criterion in Eqn. 2 through this parameter space. In Fig. 1b, we show that along paths of constant $\mathcal{S}$, Ro decreases as a function of Ra and Ta. Along paths of constant Co, Ro increases with increasing Ra and Ta. However, along paths of constant $\mathcal{P}_{\mathrm{Ro}}$, after an increase at low Ra, the evolved value of Ro levels off and stays roughly constant as a function of Ra. Holding $\mathcal{P}_{\mathrm{Ro}}$ constant seems to predict Ro relatively well from our experimental trials here, particularly at low Ro. In Fig. 1c, we show how the Ro varies as a function of $\mathcal{P}_{\mathrm{Ro}}$ at constant supercriticality. We expect the scaling law for $\mathrm{Ro} \leq 0.4$ to hold up to low Ro, and the leveling off seen at higher Ro and higher $\mathcal{P}_{\mathrm{Ro}}$ is likely influenced by the curvature of the supercriticality curve at low Ra and Ta (see Fig. 1a).

We define the Nusselt number (Nu, which quantifies heat transport in a convective solution) as we did previously in AB17. In Fig. 3a, we show the scaling of Nu as a function of Ra at fixed $\mathcal{P}_{\mathrm{Ro}}$. We find that when $\mathcal{P}_{\mathrm{Ro}}$ is held constant and Ra is increased, we find a scaling of $\mathrm{Nu} \propto \mathrm{Ra}^{0.27}$, which is reminiscent of classical scaling laws in non-rotating theory, and suggests that changes in heat transport along these paths are boundary driven. Furthermore, in Fig. 3b, we plot the RMS Reynold's number ($\mathrm{Re} = |u|L_z/\nu$) as a function of Ra, and find that $\mathrm{Re} \propto \mathrm{Ra}^{1/2}$, which is precisely the scaling we found in the non-rotating regime in AB17.

In Fig. 2, we show sample snapshots of the convective flows in our domain. I'll need to talk about them once I get there.

In Fig. 4, we show time- and horizontally-averaged profiles of the rossby number and the entropy gradient.

[1] http://dedalus-project.org/

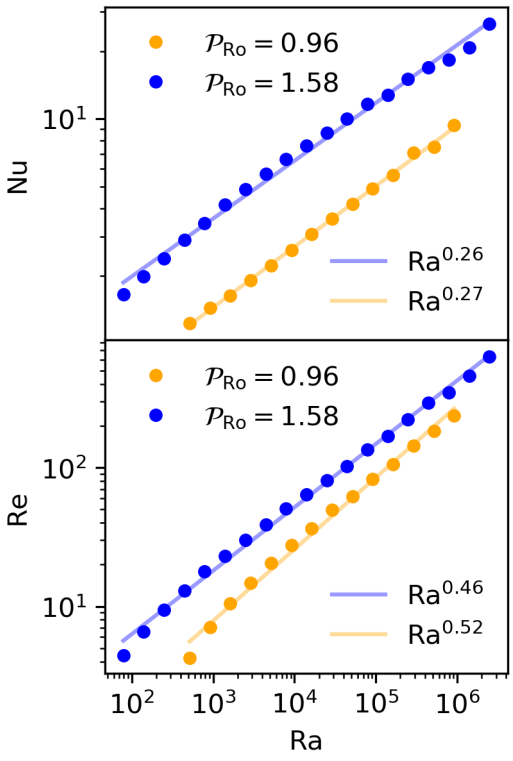

Figure 3. (a) Evolved Nu vs. Ra along constant $\mathcal{P}_{\rm Ro}$ paths. A scaling law of $Nu \propto Ra^{0.27}$ is observed, which is very similar to classic scaling laws. (b) Evolved Re vs. Ra along constant $\mathcal{P}_{\rm Ro}$ paths. A classic scaling law of $Re \propto Ra^{1/2}$ is observed. The similarity between these laws and classical laws in Rayleigh-Bénard convection suggests that at fixed $\mathcal{P}_{\rm Ro}$, varying Ra affects the evolved dynamics in a manner similar to a nonrotating fluid.

As Ra increases at a constant value of $\mathcal{P}_{\rm Ro}$, both the entropy and rotational boundary layers shrink. We measure the upper boundary layer thicknesses of both profiles. We measure the boundary layer thickness of the Rossby number as the distance from the upper boundary to the point at which Ro is maximized. We measure the boundary layer thickness of the entropy profile by fitting a line to the upper 10 points in the domain, and assuming that the boundary layer extends to the point at which that line crosses through zero. We plot $\delta_S/\delta_{\rm Ro}$ as a function of Ra for our $\mathcal{P}_{\rm Ro}$ paths in Fig. 4b. We find that the ratio of these boundary layers is relatively constant as a fucntion of Ra, which implies that the rotational constraint across Ra is roughly constant. [NOTE: NEED TO TALK ABOUT MAGNITUDE OF RO IN BOUNDARY LAYER]

4. DISCUSSION

In this letter, we studied rotating, stratified, compressible convection at low Mach number. We studied traditional paths through Ra-Ta space, as well as a new path, in which the Predictive Rossby number, $\mathcal{P}_{\rm Ro}$, is held constant, and $\mathrm{Ra} = \mathcal{P}_{\rm Ro}\,\mathrm{Ta}^{3/4}$. Along these paths, we find that the evolved rotational constraint, as measured by the Rossby number (Ro), is roughly constant as Ra increases. Furthermore, the heat transport, measured by the Nusselt number (Nu), and the level of turbulence, as measured by the Reynolds number (Re), vary according to traditional scaling laws as Ra increases. Together, these phenomena suggest that experimenters in stratified convection can specify the degree of rotational constraint in their evolved solutions by choosing $\mathcal{P}_{\rm Ro}$, and then increase Ra in a manner analogous to unrotating convection (e.g., AB17) to increase the efficiency and turbulent nature of the convective dynamics in question.

4.1. *acknowledgements*

EHA acknowledges the support of the University of Colorado's George Ellery Hale Graduate Student Fellowship. This work was additionally supported by NASA LWS grant number NNX16AC92G. Computations were conducted with support by the NASA High End Computing (HEC) Program through the NASA Advanced Supercomputing (NAS) Division at Ames Research Center on Pleiades with allocations GID s1647.

REFERENCES

Anders, E. H., & Brown, B. P. 2017, Physical Review Fluids, 2, 083501

Augustson, K. C., Brown, B. P., Brun, A. S., Miesch, M. S., & Toomre, J. 2012, ApJ, 756, 169

Aurnou, J. M., & King, E. M. 2017, Proceedings of the Royal Society of London Series A, 473, 20160731

Brown, B. P., Browning, M. K., Brun, A. S., Miesch, M. S., & Toomre, J. 2008, ApJ, 689, 1354

—. 2010, ApJ, 711, 424

Brown, B. P., Miesch, M. S., Browning, M. K., Brun, A. S., & Toomre, J. 2011, ApJ, 731, 69

Brummell, N. H., Hurlburt, N. E., & Toomre, J. 1996, ApJ, 473, 494

—. 1998, ApJ, 493, 955

Busse, F. H. 2002, Physics of Fluids, 14, 1301

Calkins, M. A., Julien, K., & Marti, P. 2015, Geophysical and Astrophysical Fluid Dynamics, 109, 422

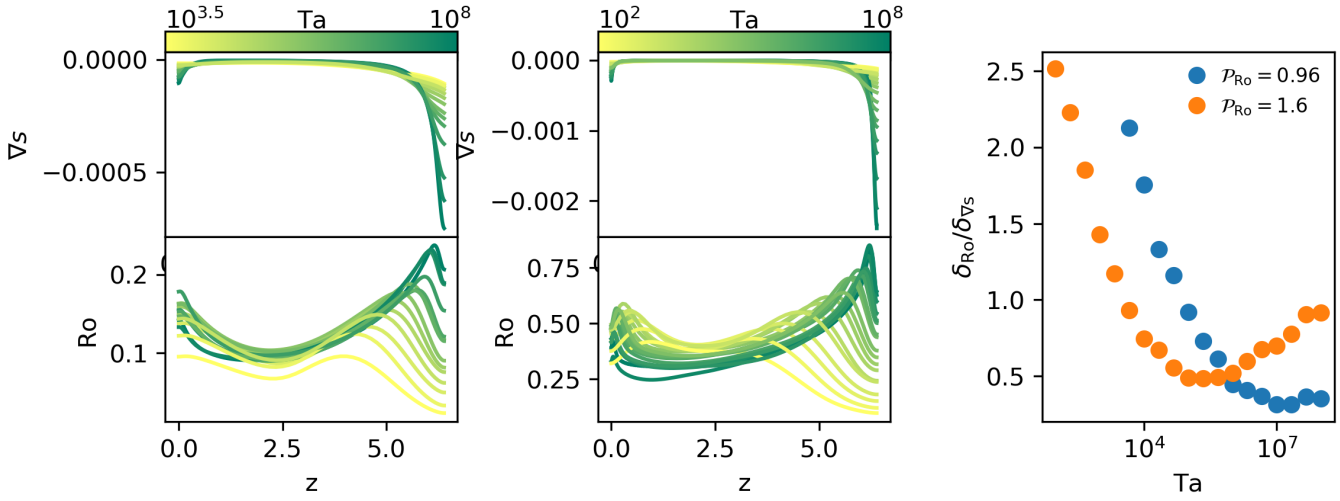

Figure 4. (a) Horizontally-averaged profiles of the Rossby number are shown vs. z for a constant $\mathcal{P}_{\mathrm{Ro}}$ = X. (b) Horizontally-averaged profiles of the entropy gradient are shown vs. z for a constant $\mathcal{P}_{\mathrm{Ro}}$ = X. (c) Vorticity boundary layer thickness normalized by entropy boundary layer thickness as a function of Ta/Ta_crit for multiple $\mathcal{P}_{\mathrm{Ro}}$ paths. When this measure is $\gg 1$, we expect the flows to be buoyancy dominated, when it is $\ll 1$, we expect the flows to be rotationally dominated, and when it is ~ 1, we anticipate that both effects are very important.

Featherstone, N. A., & Hindman, B. W. 2016, ApJ, 830, L15

Glatzmaier, G. A., & Gilman, P. A. 1982, ApJ, 256, 316

Greer, B. J., Hindman, B. W., Featherstone, N. A., & Toomre, J. 2015, ApJL, 803, L17

Greer, B. J., Hindman, B. W., & Toomre, J. 2016, ApJ, 824, 4

Guerrero, G., Smolarkiewicz, P. K., Kosovichev, A. G., & Mansour, N. N. 2013, ApJ, 779, 176

Hanasoge, S. M., Duvall, T. L., & Sreenivasan, K. R. 2012, Proceedings of the National Academy of Science, 109, 11928

Julien, K., Knobloch, E., Rubio, A. M., & Vasil, G. M. 2012, Physical Review Letters, 109, 254503

Julien, K., Legg, S., McWilliams, J., & Werne, J. 1996, Journal of Fluid Mechanics, 322, 243

Käpylä, P. J., Käpylä, M. J., & Brandenburg, A. 2014, A&A, 570, A43

King, E. M., Stellmach, S., Noir, J., Hansen, U., & Aurnou, J. M. 2009, Nature, 457, 301

Soderlund, K. M., Sheyko, A., King, E. M., & Aurnou, J. M. 2015, Progress in Earth and Planetary Science, 2, 24

Stevens, R. J. A. M., Zhong, J.-Q., Clercx, H. J. H., Ahlers, G., & Lohse, D. 2009, PhRvL, 103, 024503

Zhong, J.-Q., Stevens, R. J. A. M., Clercx, H. J. H., et al. 2009, Physical Review Letters, 102, 044502